

Article

Efficiency Analysis of Low Electric Power Drives Employing Induction and Synchronous Reluctance Motors in Pump Applications

Vadim Kazakbaev ^{1,2,*} , Vladimir Prakht ^{1,2}, Vladimir Dmitrievskii ^{1,2},
Mohamed N. Ibrahim ^{3,4,5} , Safarbek Oshurbekov ¹ and Sergey Sarapulov ¹

¹ Department of Electrical Engineering and Electric Technology Systems, Ural Federal University, Yekaterinburg 620002, Russia; va.prakht@urfu.ru (V.P.); vladimir.dmitrievsky@urfu.ru (V.D.); s.oshurbekov@mail.ru (S.O.); s.f.sarapulov@urfu.ru (S.S.)

² EMACH LLC, Yekaterinburg 620002, Russia

³ Department of Electrical Energy, Metals, Mechanical Constructions and Systems, Ghent University, 9000 Ghent, Belgium; m.nabil@ugent.be

⁴ Core lab EEDT-MP, Flanders Make, the strategic research centre for the manufacturing industry, Gaston Geenslaan 8, 3001 Leuven, Belgium

⁵ Electrical Engineering Department, Kafrelshiekh University, Kafrelshiekh 33511, Egypt

* Correspondence: vadim.kazakbaev@urfu.ru; Tel.: +7-343-375-45-07

Received: 3 March 2019; Accepted: 21 March 2019; Published: 24 March 2019



Abstract: Due to the rapid increase in the number of variable speed AC drives, the analysis of their energy efficiency has become highly essential. However, such an analysis requires consideration of a wide variety of factors. This includes considering the energy loss in the frequency converter, depending on the motor type. In this article, a computational comparison of the energy properties of variable frequency pump drive employing two types of electric machines, i.e. an induction and a synchronous reluctance motor, is presented. The effect of the motor type on the losses in a low-voltage two-stage frequency converter using analytical and numerical models, with a further comparison, is investigated. Furthermore, an alternative approach to determine the current magnitude and power factor of the load of the converter is suggested. Eventually, this study provides a quantitative estimate of the increase in losses in the converter caused by using the two different motor types. Several experimental tests are conducted on induction and synchronous 1.1 kW reluctance motors.

Keywords: analytical models; efficiency; induction motor drive; losses; numerical models; synchronous reluctance motor drive

1. Introduction

In the recent years, improving the energy efficiency of variable speed electric drives has received a great attention; this is because the electric motors consume about 70% of industrial electricity and about 40%–45% of produced electricity [1–3]. Therefore, the necessity for efficient electric drives has become essential in many countries in the world to reduce the energy consumption and hence the environmental impact. One of the first considerable practical steps was proposing the so-called “International Energy Efficiency (IE) Classes of electric motors”, and the legislative restriction of the use of low IE-class motors [1]. To this aim, IE 60034-30-1-classes were introduced for direct-on-line (DOL) motors in which general purpose induction motors (IMs) occupy the majority of various industrial applications. In addition, IE 60034-30-2-classes were also introduced for electric motors supplied by a frequency converter (FC). Such machines include synchronous motors without starting winding (synchronous reluctance motor, permanent magnets motors, and synchronous machines with DC field

windings) and IM supplied by a FC [2]. In some applications, the potential for energy saving when using the most advanced electric drive systems, as compared with the solutions already installed, could reach 60% [3]. One of the areas with the highest potential of energy saving is mechanisms such as pumps, fans, blowers and compressors [4].

In addition, the increase in the energy efficiency of a variable speed drive can be achieved by increasing the efficiency of the frequency converter and/or the complete “power drive system” (PDS) as a whole (motor + FC). The IE classes of the converters and IES classes of the complete PDS are defined in IEC 61800-9-2 [5,6]. This standard also uses the term “complete drive module” (CDM) which includes FC, as well as additional peripheral devices such as electromagnetic compatibility filters [5]. In order to determine the IE class of FCs, IEC 61800-9-2 suggests a number of methods, among them an analytical loss model in FCs.

Recently, some research work has been devoted to the comparative analysis of various types of electric motors in variable speed drive applications [7–9]. Among other types of motors, induction motors (IMs) and synchronous reluctance motors (SynRMs) have received considerable attention.

IM and SynRM have some advantages such as the absence of brush contact, permanent magnets, simple and reliable construction, and the relatively low cost. In literature, the comparison between IM and SynRM was most often based on torque capability, overload capacity, overheating, and energy characteristics at the rated load [10–12]. Besides, conclusions about the advantages to a certain motor type could vary depending on the features of the application under consideration. Thus in reference [13] IM and SynRM are compared for use in electric transport. In references [14,15], IM and SynRM are compared for drives used in spindles and actuators. In references [7,9], IM and SynRM are compared in applications of pump systems.

However, a quantitative assessment of the influence of the motor type on the losses level in a FC lacks some research work. Consequently, this article deeply investigates a quantities assessment of the motor type on the losses level of FCs. To this end, two widely used types of electric motors in pump applications are studied i.e. induction and synchronous reluctance motors.

For this purpose, the loss models of the different components of the system (inverter, motor and pump) are necessary. The literature describes several analytical and numerical models for loss calculations [5,16–21]. The advantages of the analytical approach are the short calculation time, the visibility of the parameters dependencies and the ease of integration with other models when calculating the characteristics of a more complex system. The numerical models allow considering the nonlinear characteristics of the FC elements and the current and temperature influences on the behavior of the semiconductor elements. In addition, they also facilitate considering the design properties and modulation algorithm of the inverter.

For the inverter loss model, a limitation of the analytical model described in the IEC 61800-9-2 standard [5] is improved and then used in this article. The model of reference [5] does not take into account some design features of the implemented FC such as the big difference between the rated motor current and the rated current of the IGBT module. In addition, IEC 61800-9-2 considers the DC-capacitors losses that are caused only by the rectifier stage but not the inverter stage of FC. In this work the DC-capacitors losses caused by the inverter stage of FC are also considered.

Besides, to estimate the errors of the improved analytical method, a proposed numerical model is also implemented, as can be seen later. Although it is more common to use SPICE software to determine losses in electronic systems, in this work Matlab-Simulink software is used as a general and fast solution that can be easily integrated with more complex systems.

Moreover, the results of losses calculation using the analytical model were compared with losses measured in an experiment.

To study the behavior of an electric drive in pump applications, the researchers often use the assumption of an ideal pump load characteristic ($T \sim n^2$, where T is torque on the motor shaft; n is rotational speed of the motor) [8]. However, the actual $T(n)$ profile of the pump load is significantly different from the ideal case. The references [4,7,9] demonstrate the importance of using the pump

unit model for a specific application which is based on either experimental or statistical data. In this article, a semi-analytical model based on the catalogue data [22] and the data of the load cycle of the pump unit [9] are used to calculate the accurate T - n characteristic of the pump.

The characteristics of the various types of motors in this work is carried out based on experimental data obtained at the 7 standard operating points according to IEC 61800-9-2 [5]. To evaluate the characteristics of the motor in the loading points of the operating cycle of the mechanism, a polynomial interpolation of those data is done [9,23]. Moreover, to improve the models of reference [5], the authors in this article suggest applying interpolation not only to the data on the motor efficiency, as described in reference [5,9,23], but also to the data on its current and power factor values, to calculate losses in the FC. This approach is more accurate and general than the indirect determination of these values, based on the relative values of the motor torque and the apparent power of the FC, as proposed in reference [5]. Moreover, this approach does not require additional motor tests. Only tests in the 7 load operating points according to reference [5] are required.

Eventually, a quantitative estimation of the increase in losses in the frequency converter when using SynRM is investigated compared with that of IM.

2. Evaluation of the Performance of the Pump and Motors

The complete structure of the investigated system consists of the pump, motor and the frequency converter as sketched in Figures 1 and 2. In order to compute the T - n (torque-speed) characteristics of the pump unit, the hydraulic load settings, which are the fluid flow rate (Q) and the hydraulic head (H), are necessary. Using those load settings, the input power of the pump can be known, hence the required motor output power. Eventually, using the solution of the complete drive models, the input power from the grid to the converter can be obtained, resulting in an estimation for the losses. Notice that, the direction of the arrows in Figure 1 shows the direction of the input power calculation. However, the direction of the power flow is of course starting from the grid (P_1) to the load. Two types of electric motors to drive the pump are considered in this study: the induction motor (IM) and the synchronous reluctance motor (SynRM), having a rating output power of 1.1 kW.

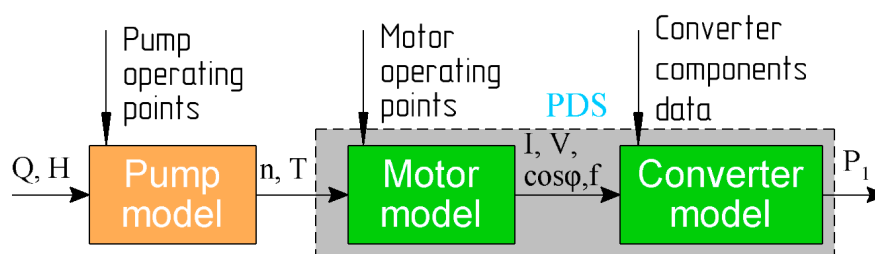


Figure 1. General structure of the whole drive system.

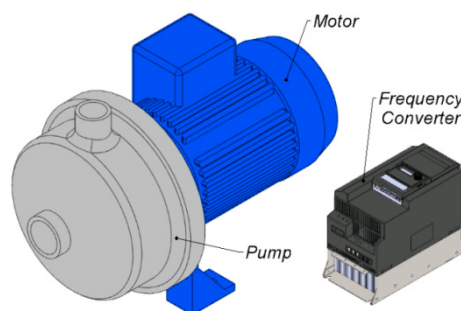


Figure 2. Sketch of the pump unit.

2.1. Evaluation of the Pump Performance

The NM 40/12F/A centrifugal pump is used in this work with the specifications given in Table 1 (manufactured by Calpeda) [22]. Table 1 shows the characteristics of the pump referring to the best efficiency point (BEP) at the rated speed at which the flow rate $Q_{rate} = 24 \text{ m}^3/\text{hour}$, the hydraulic head $H_{rate} = 11 \text{ m}$, the efficiency $\eta_{BEP} = 72\%$ and the shaft power $P_2 = 999 \text{ W}$. The data of Table 1 is then used to obtain the H - Q curve of the pump.

Table 1. Specifications of the 1.1 kW NM 40/12F/A Pump at the rated speed of 2900 rpm.

Q/Q_{BEP}	H/H_{BEP}	$\eta_{pump}, \%$	P_2/P_{2BEP}
0.75	1.09	68.2	0.863
1	1	72.0	1
1.1	0.96	70.9	1.072

This pump unit is assumed to operate continuously with the hydraulic load $H(Q)$ typical as the HVAC (Heating, Ventilation, Air Conditioning) applications [4]. To simplify the calculation, the entire working cycle of the pump is represented by 4 modes as listed in Table 2. During the day, the consumption amount will vary from 100% ($24 \text{ m}^3/\text{hour}$, $t_i/t_\Sigma = 6\%$ of the full day, where t_Σ is the total operating time and equals 24 h, t_i is the pump time of operation in this mode) up to 25% ($6 \text{ m}^3/\text{h}$, $t_i/t_\Sigma = 44\%$ of the full day). The required head, in this case, varies linearly: from the rated value to half of the rated value at zero flow rate [9]. Table 2 shows the results of the 4 modes of the pump unit operation calculated using the method described in reference [9], taking into account the aforementioned assumptions.

Table 2. Pump and motor load cycle.

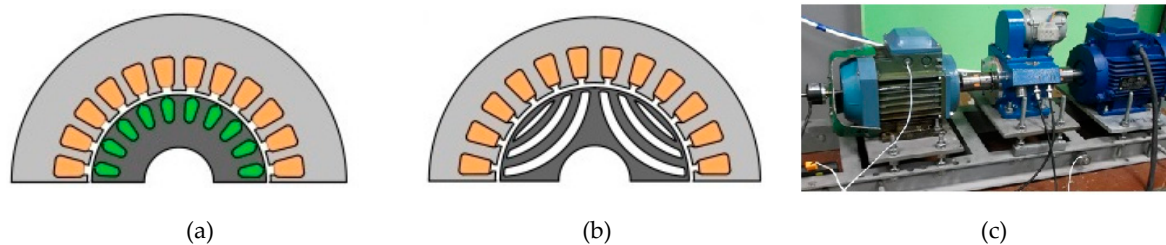
Mode No.	$t_i/t_\Sigma \%$	$Q, \%$	$H, \%$	P_2, W	n, rpm	$T, \text{N}\cdot\text{m}$
1	44	25	62.5	345.712	2108.3	1.566
2	35	50	75	490.591	2380.9	1.968
3	15	75	87.5	692.423	2644.8	2.500
4	6	100	100	999.167	2900	3.290

2.2. Evaluation of the Motor Performance

In this section, the methodology for the performance assessment of the IM and the SynRM as a part of the pump unit is presented. The examined machines are of the general-purpose type, with the rated power and speed of 1.1 kW and 3000 rpm respectively. Both the IM and the SynRM have a similar housing. The IM is a commercially motor of IE3 class. The SynRM prototype of reference [24] is used. More detailed data of the motors are presented in Table 3. Figure 3a,b shows a sketch for the motors geometry.

Table 3. Dimensions, mass and cost of the active materials of 1.1 kW, 3000 rpm motors.

Parameter	IM	SynRM
IEC Frame Size	80	80
Stator outer diameter, mm	125	125
Stack length, mm	78	70
Number of electric poles	2	4
Air gap, mm	0.3	0.28
Copper, kg	1.45	1.85
Steel, kg	5.34	3.75
Aluminum (Squirrel cage), kg	0.37	-
Mass of active materials, kg	7.16	5.60
Motor weight with housing, kg	11.0	9.5
Copper, \$	10.13	12.95
Steel, \$	5.34	3.75
Aluminum (Squirrel cage), \$	0.74	-
Price of active materials, \$	16.22	16.70

**Figure 3.** (a) Sketch of IM geometry; (b) Sketch of SynRM geometry; (c) The experimental test bench.

Due to the slip, the IM has the rated speed 2875 rpm (not 3000 rpm) and the rated torque of 3.65 N·m (not 3.5 N·m) according to its nameplate. However in this study the IM was tested as a motor with rated values of 1.1 kW and 3000 rpm; this is done using the control system.

Electrical parameters of the motors are presented in the table. Parameters of the SynRM were measured during the tests. Parameters of the IM were calculated on the basis of the manufacturer's test report [25].

The number of poles is 4 for SynRM however, IM of 2 poles used because a general purpose frequency-controlled 4-pole IM with the rated speed of about 3000 rpm is still a very rare product on the market. If 4-pole IM is used compared to 4-pole SynRM, the difference in efficiency of the motors would be lower than using 2-pole IM.

The motor characteristics in the required operating modes (Table 2) are estimated based on experimental measurements according to IEC 60034-30-2. The motors are tested when they were powered by FCs, using the "direct" method, according to reference [26]. The switching frequency of the inverter is 4 kHz, which is a standard switching frequency range for testing motors of the low rated power range [26]. The standard voltage/frequency ($V/f = \text{constant}$) control method is used while testing the IM [5]. Notice that the efficiency of the IM could be a slightly better in the underload operating points in case of applying a more comprehensive control strategy with a flux optimization method than the voltage/frequency ($V/f = \text{constant}$) control. However, the voltage/frequency ($V/f = \text{constant}$) strategy is the most widespread case in the industry. The SynRM is driven using a sensorless control method provided by the serially produced FC of reference [27]. In both motors, a given constant torque reference of the load machine was set during the test. A mechanical speed value needed was achieved by adjusting the frequency reference of a tested motor.

Figure 3c shows a photograph of the experimental test bench. In this work, to provide a correct comparison between the energy characteristics, the losses of the IM and the SynRM drives were interpolated using the standard method IEC 60034-30-2 when they are powered by a frequency

converter. The obtained experimental measurements of the IM and the SynRM are listed in Table 4 at several operating points of speed and torque.

Table 4. Experimental measurements of the performance of the IM and the SynRM at several operating points of speed and torque (100% of T equals to 3.5 N·m; 100% of n equals to 3000 rpm).

Operating Point	n , %	T , %	I_{out} , A (IM)	I_{out} , A (SynRM)	$\cos\varphi$ (IM)	$\cos\varphi$ (SynRM)	η_{motor} (IM)	η_{motor} (SynRM)
1	90	100	2.427	3.230	0.774	0.726	0.807	0.898
2	50	100	2.396	3.138	0.811	0.745	0.719	0.867
3	90	50	1.811	2.068	0.545	0.725	0.786	0.900
4	50	50	1.786	2.014	0.572	0.738	0.723	0.884
5	25	100	2.416	3.082	0.877	0.772	0.542	0.785
6	50	25	1.645	1.310	0.367	0.703	0.627	0.892
7	25	25	1.709	1.274	0.417	0.717	0.497	0.851

The IEC 60034-30-2 standard requires manufacturers to declare motor efficiency values at 7 operating points (Table 4). Some manufacturers provide such data in their catalogues [28]. However, the measurements given in Table 4 demonstrate that only η_{motor} data is insufficient for calculating the losses in the FC and in the drive as a whole. It is also necessary to know the current and power factor. To deal with this problem, the IEC 61800-9-2 standard proposes making look-up tables with loss values in CDM depending on “relative torque producing current ($I_r, torque$)” and “relative motor stator frequency”, as well as reference tables with I_{out} ($I_r, torque, S_r, equ$) and $\cos\varphi$ ($I_r, torque, S_r, equ$); where S_r, equ is the rated apparent power of the CDM [5]. However, this solution is applicable only for calculating the efficiency of a drive with IM having typical parameters. To apply this approach to other types of motors (in particular to SynRM), it is necessary to compile reference tables I_{out} ($I_r, torque, S_r, equ$) and $\cos\varphi$ ($I_r, torque, S_r, equ$), that are applicable with sufficient accuracy for each type of motor.

Consequently, we propose a more general and accurate approach using the 7 standard points of I_{out} and $\cos\varphi$ values obtained during the tests in addition to the data on the η_{motor} . The inclusion of these data in the motor technical documentation does not require additional tests, besides those necessary for measuring motor efficiency at 7 points, according to IEC 61800-9-2. As this is already specified for η_{motor} [28], the manufacturers can declare the values of I_{out} and $\cos\varphi$ at no additional cost in the technical documentation. Therefore, this approach could be promising.

Moreover, the obtained measurements of Table 4 are used to calculate the coefficients of second order interpolating polynomials $f(T, n)$, according to [5,23]:

$$A = X^{-1} \cdot B, \text{ i.e. } \begin{bmatrix} a_1 \\ a_2 \\ a_3 \\ a_4 \\ a_5 \\ a_6 \\ a_7 \end{bmatrix} = \begin{bmatrix} n_1 & n_1^2 & n_1 \cdot T_1^2 & n_1^2 \cdot T_1^2 & T_1^2 & T_1 & 1 \\ n_2 & n_2^2 & n_2 \cdot T_2^2 & n_2^2 \cdot T_2^2 & T_2^2 & T_2 & 1 \\ n_3 & n_3^2 & n_3 \cdot T_3^2 & n_3^2 \cdot T_3^2 & T_3^2 & T_3 & 1 \\ n_4 & n_4^2 & n_4 \cdot T_4^2 & n_4^2 \cdot T_4^2 & T_4^2 & T_4 & 1 \\ n_5 & n_5^2 & n_5 \cdot T_5^2 & n_5^2 \cdot T_5^2 & T_5^2 & T_5 & 1 \\ n_6 & n_6^2 & n_6 \cdot T_6^2 & n_6^2 \cdot T_6^2 & T_6^2 & T_6 & 1 \\ n_7 & n_7^2 & n_7 \cdot T_7^2 & n_7^2 \cdot T_7^2 & T_7^2 & T_7 & 1 \end{bmatrix}^{-1} \cdot \begin{bmatrix} b_1 \\ b_2 \\ b_3 \\ b_4 \\ b_5 \\ b_6 \\ b_7 \end{bmatrix}, \quad (1)$$

where A is the 7×1 coefficient vector to be found; X is the 7×7 variable (T and n) matrix; B is the 7×1 answer vector (for example it may consist of given values of motor current). As such, the value of a considered operating characteristic of the motor can be found by:

$$b(T, n) = a_1 \cdot n + a_2 \cdot n^2 + a_3 \cdot n \cdot T^2 + a_4 \cdot n^2 \cdot T^2 + a_5 \cdot T^2 + a_6 \cdot T + a_7, \quad (2)$$

where $b(T,n)$ is the variable value to be found (motor current, efficiency or power factor); a_1 to a_7 are the elements of the coefficient vector A .

The calculated motor performances obtained on the basis of data in Table 4 using the interpolation procedure (2) for the pump operating modes under consideration (Table 2) are presented in Table 5. Tables 4 and 5 have the following designation for motor characteristics: I_{out} is the RMS phase current; V_{out} is the RMS phase voltage; $\cos\phi$ is the power factor; P_{1ph} is the phase active power; f is the electrical frequency of the fundamental harmonic; η_{motor} is the motor efficiency. It can be noted that the value of η_{motor} for SynRM in all the considered modes is higher than that of IM.

Table 5. Performance of motors during the pump operating points of Table 2.

Mode No.	IM						SynRM					
	I_{out}, A	V_{out}, V	$\cos\phi$	P_{1ph}, W	f, Hz	η_{motor}	I_{out}, A	V_{out}, V	$\cos\phi$	P_{1ph}, W	f, Hz	η_{motor}
1	1.742	168.3	0.512	150.0	35.1	0.768	1.902	92.4	0.726	127.6	70.28	0.903
2	1.844	189.6	0.587	205.2	39.7	0.797	2.218	111.9	0.730	181.1	79.36	0.903
3	2.017	210.7	0.672	285.5	44.1	0.808	2.607	134.5	0.732	256.6	88.16	0.900
4	2.344	223.7	0.766	414.8	48.3	0.808	3.124	163.6	0.731	373.4	96.67	0.892

In this case the motor $\cos\phi$ is calculated as the following:

$$\cos\phi = \frac{3 \cdot P_{1ph}}{\sqrt{3} \cdot V_{rms\ line\ fund} \cdot I_{out}}, \quad (3)$$

where $V_{rms\ line\ fund}$ is the RMS value of waveform of the measured motor line voltage averaged over the PWM period.

In addition, Table 5 shows performance of the motors when loaded by the pump at the given conditions of Table 2. Notice that the frequency values f of the IM are calculated without taking the rotor slip into account. This is an assumption of the proposed method. But it does not produce a significant error in the computed losses of FC.

Using Equation (2) for mode No. 4 in Table 2, we obtain the following results: $I_{out} = 2.344$ A, $V_{out} = 231$ V, $\cos\phi = 0.761$, $P_{1ph} = 412$ W. However, it must be taken into account that the actual maximum output voltage of FC is slightly lower than the theoretical limitation given by the inverter modulation index.

The modulation index for the inverter for the case of the space vector modulation (SVM) is calculated by [17,18]:

$$m = \frac{\sqrt{3} \cdot V_{m\ phase\ fund}}{V_{DC}}, \quad (4)$$

where $V_{m\ phase\ fund} = \sqrt{2} \cdot V_{out}$ is the amplitude of the modulated phase voltage of the load; V_{DC} is DC-link voltage.

The theoretical maximum value is $m = 1$ without over modulation. The maximum value of the RMS line voltage is [17]:

$$V_{line\ fund\ rms} = \frac{V_{DC}}{\sqrt{2}}. \quad (5)$$

In this work, all calculations are conducted for the case of the symmetrical space vector modulation. Thus, if V_{DC} equals 565 V, then the theoretical maximum effective linear voltage is 400 V and the limitation of phase voltage is 231 V. However, there are additional hardware limitations of maximum PWM duty cycle due to the presence of dead time and the restricted switching speed of IGBT drivers. Therefore, the maximum modulation index of the FC that was under testing in this work is about 97%.

Considering this, we assume $V_{out} = 0.97 \cdot 231 = 227.8$ V in mode No. 4 for IM. In addition, according to reference [5], an increase in IM losses caused by the FC voltage drop (motor de-fluxing) was calculated:

$$P_{motor\ loss}' = \frac{V_{out}}{V_{out\ max\ CDM}} \cdot P_{motor\ loss}, \quad (6)$$

where V_{out} is the value of motor voltage obtained using (2); $P_{motor\ loss} = P_1 - P_2$ is the value of motor losses obtained using (2); $V_{out\ max\ CDM} = 227.8$ V is the maximum output CDM voltage.

The increase in motor losses also causes an increase in $\cos\varphi$. With this we assume that the value of I_{out} remains the same since there is not only an increase in the active component of the current but also a decrease in the reactive component.

To compare the cost of the considered motors, Table 3 shows an estimation of the mass and the cost of the active materials. It is observed that the costs are comparable. In addition, SynRM does not have a cast squirrel cage in the rotor, therefore its production technology is cheaper than that of IM.

3. Evaluation of the Performance of the Drive Module Components

In this section, analytical and numerical models of losses calculation of the complete drive module (CDM) are presented. In addition, the results of both models are compared.

Both IM and SynRM drives include FC with the same power electronic modules (Infineon FP25R12W2T4_B11, $I_{c\ nom} = 25$ A) [29]. This module is used for frequency converter for a power range of 0.75–7.5 kW by several manufacturers, e.g. in reference [27].

The modern two-stage low-voltage FC consists of several separate electronic and passive electrical components. It is accepted that the losses in different parts of the FC are calculated independently [5]. To consider the mutual influence of individual components, it is possible to use iterative procedures [21]. According to reference [5], the following types of losses are distinguished in CDM:

- Losses in the inverter;
- Losses in the rectifier;
- Losses in the input choke (if the choke is used); in the considered case the choke is not applied;
- Losses in DC-link;
- Losses in current-carrying buses (relevant only for FCs of a high power);
- Losses in the control system;
- Losses in the cooling system.

The losses of the different components in the CMD are calculated by analytical and numerical models as follows:

3.1. Analytical Model of the Losses in CDM

3.1.1. Inverter Losses

Figure 4a shows a 3-phase IGBT inverter circuit. Each switch consists of the IGBT transistor and the reverse diode connected in parallel. The losses in the inverter switches are divided into the conduction and switching losses. In addition, they can be divided into losses in IGBT and in reverse diodes [16,18].

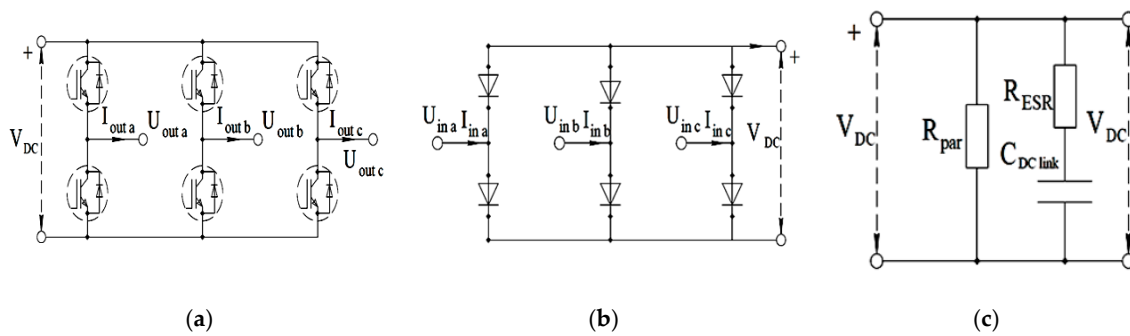


Figure 4. Electrical schemes of the models: (a) three-phase inverter; (b) three-phase uncontrolled rectifier (passive rectifier bridge); (c) DC-link.

The processes occurring in each phase of the three-phases of the inverter are similar in the steady state. This makes it possible to consider the processes only in one of the phases. Losses in the ON state of the module depend mainly on the magnitude of the current (i.e., on the amplitude, if the PWM current ripple is neglected) [18].

Figure 5a shows the forward V - I characteristics of the elements of the electronic module under consideration: IGBT, the reverse diode, and the rectifier diode [29]. It is clear that $\Delta u(i)$ is non-linear in the range of permissible currents. To use simple analytical expressions in the calculation, it is usually proposed to present the voltage drop across the element $\Delta u(i)$ using a linear relation constructed from two points [5,16,18]. To increase the accuracy of the analytical calculation for the cases under consideration, (the amplitude of the phase current of the motor $I_m < 6$ A, see Table 5), it is reasonable to use two points on the linear sections of $\Delta u(i)$ dependences (Figure 5b) at $I_m < 6$ A, but not at the high range of currents.

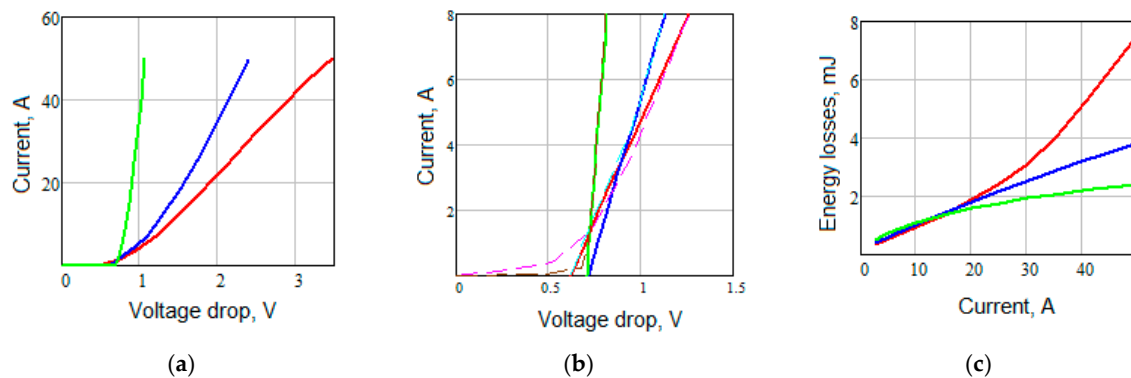


Figure 5. (a) Direct current-voltage characteristics of semiconductor elements [29]; red—IGBT; blue—reverse diode; green—uncontrolled rectifier diode; (b) solid line—linear approximation of (a); dotted line—source dependencies; (c) Dependence of switching losses on current [29] at rated voltage IGBT of the V_{rate} module; red—IGBT turn on; blue—IGBT turn off; green—reverse diode turn off.

According to the data from reference [29], the following parameters were calculated in Table 6:

Table 6. Parameters from the IGBT and diodes I - V forward curves.

Linearized Conduction Losses	Value
U_{Tth} (IGBT threshold voltage), V	0.615
R_{Tfs} (IGBT forward slope resistance), m Ω	81
U_{Dth} (reverse diode threshold voltage), V	0.715
R_{Dfs} (reverse diode forward slope resistance), m Ω	52
U_{Drth} (rectifier diode threshold voltage), V	0.705
R_{Drfs} (rectifier diode forward slope resistance), m Ω	14

Assuming sinusoidal currents and voltages, if $\cos\varphi < 1$ (typical in case of drive applications), then during the electrical period the module output current flows not only through the transistors but also through the reverse diodes. If $U_{Tth} \neq U_{Dth}$ and $R_{Tfs} \neq R_{Dfs}$, the conduction losses is expressed by [5]:

$$\begin{aligned}
 P_{L_{on}} &= P_{L_{onT}} + P_{L_{onD}}; \\
 P_{L_{onT}} &= \sqrt{2} \cdot I_{out} \cdot U_{Tth} \cdot \left(\frac{1}{2\pi} + \frac{1.22 \cdot m \cdot \cos\varphi}{8} \right) + R_{Tfs} \cdot 2 \cdot I_{out}^2 \cdot \left(\frac{1}{8} + \frac{1.22 \cdot m \cdot \cos\varphi}{3 \cdot \pi} \right); \\
 P_{L_{onD}} &= \sqrt{2} \cdot I_{out} \cdot U_{Dth} \cdot \left(\frac{1}{2\pi} - \frac{1.22 \cdot m \cdot \cos\varphi}{8} \right) + R_{Dfs} \cdot 2 \cdot I_{out}^2 \cdot \left(\frac{1}{8} - \frac{1.22 \cdot m \cdot \cos\varphi}{3 \cdot \pi} \right),
 \end{aligned} \quad (7)$$

where $P_{L_{on}}$ is total loss in one switch in the ON-state (transistor + reverse diode); $P_{L_{onT}}$ is the losses in the ON-state in one transistor; $P_{L_{onD}}$ is the losses in the ON-state in one reverse diode; I_{out} is the RMS value of the motor phase current; $\cos\varphi$ is the load power factor, m is the modulation index.

It is often seen that $(U_{Tth} + R_{Tfs} \cdot I_{out}) > (U_{Dth} + R_{Dfs} \cdot I_{out})$ as seen in Figure 5a. Therefore, if $I_{out} = \text{const}$, then as the product $\cos\varphi \cdot m$ decreases, the conduction losses in ON-state switches decrease (the relative time of current flow through the diodes increases) [16,18]. However, the difference between U_{Tth} and U_{Dth} and between R_{Tfs} and R_{Dfs} is not so significant. As a consequence, a decrease in $\cos\varphi$ at $I_{out} = \text{const}$ for SynRM does not lead to an increase in in the inverter losses. It is observed that the effect of m and $\cos\varphi$ on the losses is much lower than the effect of the current amplitude (within 5–7% with the standard parameters of the inverter) [18]. Thus, with the use of SynRM, the main part of the loss increase in the FC is due to an increase in I_{out} . In addition, the temperature rise of the inverter switches also affects the losses.

In order to determine the switching losses, it is common to use the previously measured dependences of the energy losses on current and voltage for one switching period [17]. As a rule, these dependencies are non-linear as shown in Figure 5c. To use simple analytical formulas for these dependencies, linearization can also be used [5,16]. In this work, the switching losses are linearized over their initial approximately linear segment (Table 7).

Table 7. Parameters from the IGBT and diodes switching losses curves.

Linearized Switching Losses	Value
E_{Ton} (IGBT turn-on losses), J/A	$0.143 \cdot 10^{-3}$
E_{Toff} (IGBT turn-off losses), J/A	$0.152 \cdot 10^{-3}$
E_{Doff} (reverse diode turn-off losses), J/A	$0.204 \cdot 10^{-3}$

In the case of using the linear approximation, the switching losses are given by [5]:

$$\begin{aligned}
 P_{L_{sw}} &= P_{L_{swTon}} + P_{L_{swToff}} + P_{L_{swDoff}}; \quad P_{L_{swTon}} = \frac{E_{Ton}}{\pi} \cdot \frac{V_{DC}}{V_{rate}} \cdot f_{sw} \cdot \sqrt{2} \cdot I_{out}; \\
 P_{L_{swToff}} &= \frac{E_{Toff}}{\pi} \cdot \frac{V_{DC}}{V_{rate}} \cdot f_{sw} \cdot \sqrt{2} \cdot I_{out}; \quad P_{L_{swDoff}} = \frac{E_{Doff}}{\pi} \cdot \frac{V_{DC}}{V_{rate}} \cdot f_{sw} \cdot \sqrt{2} \cdot I_{out},
 \end{aligned} \quad (8)$$

where P_{Lsw} is the total switching losses for one switch (transistor + reverse diode); $P_{Lsw\ T\ on}$ is the turn-on losses of the transistor; $P_{Lsw\ T\ off}$ is the turn-off losses of the transistor; $P_{Lsw\ D\ off}$ is the turn-off losses of the reverse diode; f_{sw} is the PWM frequency; V_{DC} is the DC voltage of the inverter; V_{rate} is the rated reverse voltage of the IGBT module transistors.

The influence of the temperature on the inverter losses can be also taken into account by adding a thermal model. In this case, a combined solution of electrical and thermal equations is done either in calculating the dynamic equations [20] or in a simpler iterative search for the stationary values of the electrical model parameters depending on the temperature [21]. The influence of temperature on the parameters of the converter is not taken into account in this work. Hence, the parameters are calculated for a fixed temperature of 150 °C.

3.1.2. Uncontrolled Rectifier (Passive Rectifier Bridge) Losses

To determine the losses in the rectifier diodes, see Figure 4b, the same approach of the inverter conduction losses can be used. Switching losses are not taken into account, since the rectifier diodes switch with the power grid frequency of 50 Hz $\ll f_{sw}$. The direct V - I characteristic of a rectifier diode is shown in Figure 5a,b. Table 6 shows the linearized parameters of the rectifier diode. Thus, the losses in one of 6 diodes of the rectifier are computed as follows [30]:

$$P_{r\ diode} = I_{r\ av} \cdot U_{Dr\ th} + R_{Dr\ fs} \cdot I_{r\ rms}^2, \quad (9)$$

where $I_{r\ av}$ and $I_{r\ rms}$ are the average and the RMS phase currents of the rectifier.

Calculation of the $I_{r\ av}$ and $I_{r\ rms}$ values requires knowing the values of the power and form factors of the rectifier input phase current. In case of analytical calculation, it is difficult to estimate the power factor with a sufficient level of accuracy. Therefore, let us assume the input power factor $\lambda_{in} = 0.65$ [5]. Under the assumptions made, based on the law of conservation of energy (electric power balance) at the input and output of the CDM and neglecting CDM's power losses, the losses in the rectifier can be calculated by [5]:

$$P_{rect} = 6 \cdot \left(\frac{\sqrt{2}}{\pi} \cdot m \cdot \cos \phi \cdot I_{out} \cdot U_{Dr\ th} + R_{Dr\ fs} \cdot \frac{\left(\frac{m \cdot \cos \phi \cdot I_{out}}{\lambda_{in}} \right)^2}{2} \right). \quad (10)$$

3.1.3. DC-link Losses

The losses of the DC capacitors and the balancing (ballast) resistors in the DC-link, see Figure 4c, are obtained by [5]:

$$P_{L\ DC\ link} = P_{L\ par\ DC} + P_{L\ cap\ DC} = \frac{V_{DC}^2}{R_{par}} + R_{ERS} \cdot (I_{ripple\ C})^2, \quad (11)$$

where $I_{ripple\ C}$ is the RMS of AC current component through the DC-link capacitance; R_{ERS} is the equivalent active series resistance of the DC-link capacitors; R_{par} is the equivalent impedance of the balancing resistors. Let us use the approximated values of the parameters $R_{par} = 10^5$ and $R_{EMS} = 0.1$ Ohm as given in references [5,31].

The calculation of the $I_{ripple\ DC}$ value encounters some difficulties due to the fact that the ripples are caused by both the inverter and the rectifier stages of the converter [32]:

$$I_{ripple\ DC} = I_{ripple\ inv} + I_{ripple\ rect}, \quad (12)$$

where $I_{ripple\ inv}$ is the magnitude of the current ripple in the DC-link capacitance caused by the inverter stage of FC and $I_{ripple\ rect}$ is the magnitude of the current ripple caused by the rectifier stage.

In order to estimate the value of $I_{ripple\ C\ rect}$ the following expression is suggested based on the standard [5]:

$$I_{ripple\ rect} = \frac{\sqrt{3}}{1.35} \cdot \frac{m \cdot I_{out} \cdot \cos \phi}{1 + 50 \cdot k_{1\ choke}}, \quad (13)$$

where $k_{1\ choke}$ is the ratio of the impedance of the choke to the rated impedance of the CDM. The coefficient $k_{1\ choke}$ can be calculated as:

$$k_{1\ choke} = \frac{2\pi \cdot f_{net} \cdot L_{choke} \cdot I_{in}}{U_{in}}, \quad (14)$$

where f_{net} is the voltage frequency at the CDM input which equals 50 Hz, U_{in} is the rated input phase voltage of the CDM and I_{in} is the rated input phase current of the CDM.

The $k_{1\ choke}$ value is assumed to equal to zero, since an input choke is not used.

In reference [5], no method is proposed for estimating $I_{ripple\ inv}$. For this purpose, an expression of the RMS of current ripple of the PWM frequency caused by the inverter part of CDM in the case of SVM is given as follows [32]:

$$I_{ripple\ inv} = I_{out} \cdot \sqrt{2 \cdot m \cdot \left[\frac{3}{4 \cdot \pi} + \cos^2 \phi \cdot \left(\frac{\sqrt{3}}{\pi} - \frac{9}{16} \cdot m \right) \right]}. \quad (15)$$

3.1.4. Control & Cooling System Losses

Besides the losses of the power circuits, a significant part of the FC losses also occurs in the control and the ventilation systems. It is assumed in reference [5] that such losses do not depend on the load. However, those losses increase with the FC rated apparent power and with the increasing complexity of the control circuits. Thus, in a drive designed for a complex automation, which has a large number of interface modules, those losses are higher than in a simpler general-purpose drive. Several sources facilitate to estimate the approximated value of those losses, depending on the type and power rating of the FC [5,33]. In this work, for FC of 1.1 kW with a rated current of 3.4 A, we use the value of those losses ($P_{control}$) equals 14 W, according to reference [33].

3.2. Numerical Model of the Losses in CDM Using Matlab/Simulink Environment

In this part a numerical loss model of CDM based on the techniques described in reference [18,19] is implemented in MATLAB/Simulink environment. Figure 6 shows the block diagram of the simulated system. The inverter load is simulated using dynamical models of IM and SynRM.

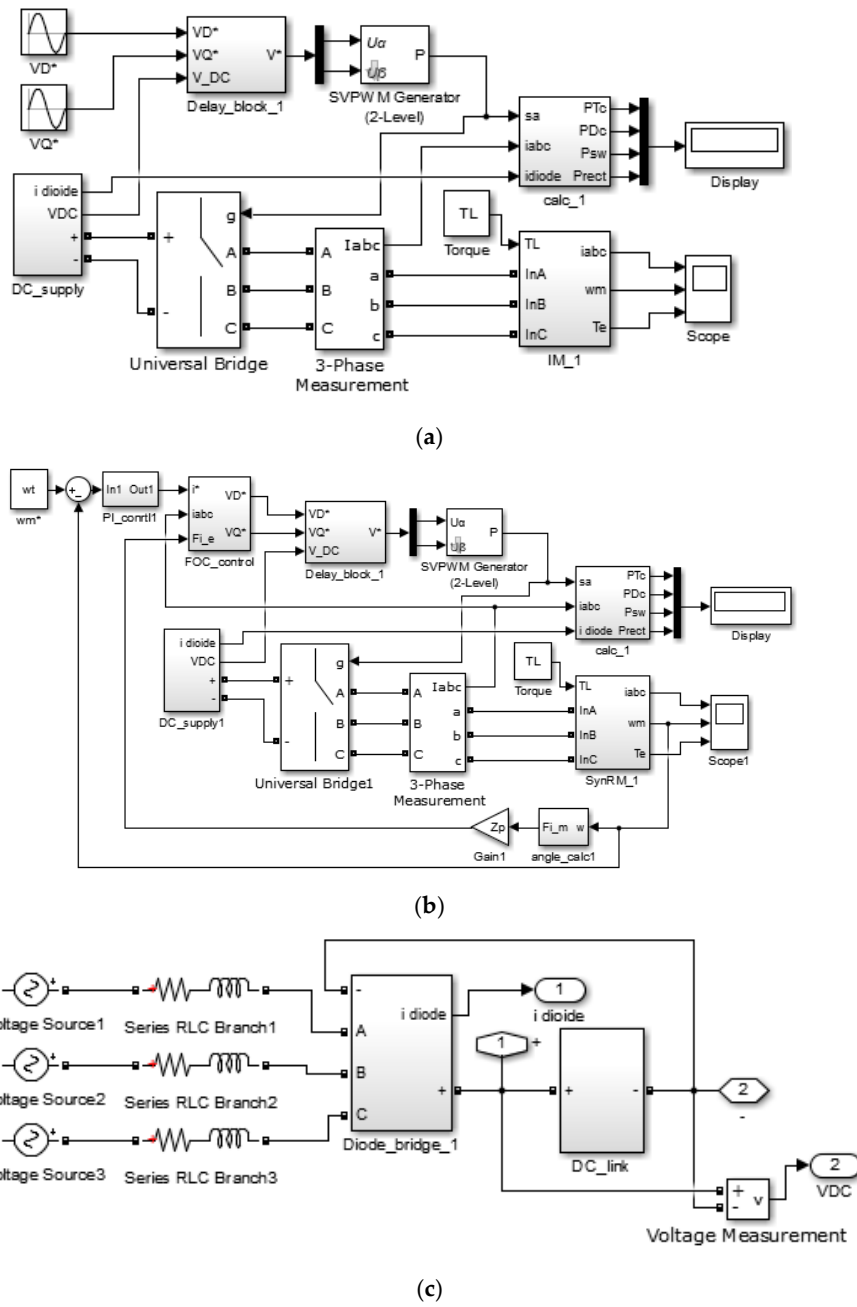


Figure 6. Simulink models. (a) CDM with IM; (b) CDM with SynRM; (c) DC supply block.

IM is modeled using equations in dq -axis frame rotating synchronously with the rotor flux vector:

$$\begin{aligned}
 T_s \cdot \frac{di_d}{dt} &= -k_r \cdot i_d + \frac{L_m \cdot R_r}{L_r^2 \cdot R_s} \cdot \lambda_r + T_s \cdot \omega_\lambda \cdot i_q + \frac{1}{R_s} \cdot v_d; \\
 T_s \cdot \frac{di_q}{dt} &= -k_r \cdot i_q - \frac{L_m}{L_r \cdot R_s} \cdot \omega_e \cdot \lambda_r - T_s \cdot \omega_\lambda \cdot i_d + \frac{1}{R_s} \cdot v_q; \\
 T_r \cdot \frac{d\lambda_r}{dt} &= -\lambda_r + L_m \cdot i_d; \\
 \omega_\lambda &= \omega_e + \omega_s = Z_p \cdot \omega_m + \frac{L_m}{T_r} \cdot \frac{i_q}{\lambda_r} = \omega_e + s \cdot \omega_\lambda; \\
 T &= \frac{3}{2} \cdot Z_p \cdot \frac{L_m}{L_r} \cdot \lambda_r \cdot i_q,
 \end{aligned}
 \tag{16}$$

where $\lambda_r = \lambda_{rd}$ is the rotor flux linkage; i_d, i_q are the stator currents (direct and quadrature components); v_d, v_q are the stator voltages, Z_p is the number of pairs of motor poles; $\omega_e = Z_p \cdot \omega_m$ is the electrical angular frequency of the rotor; ω_m is the mechanical angular frequency of the rotor; ω_λ is the angular frequency of rotor flux; s is the rotor slip; R_s is the stator resistance; R_r is the rotor resistance; L_s is the

full stator inductance; L_r is the full rotor inductance; L_m is the magnetizing inductance; T is the motor torque; $T_s = \sigma \cdot L_s / L_r$; $\sigma = 1 - L_m^2 / (L_s \cdot L_r)$; $k_r = 1 + (L_m / L_r)^2 \cdot (R_r / R_s)$; $T_r = L_r / R_r$.

SynRM is modeled using equations in dq axis frame rotating synchronously with the rotor and d -axis that is the axis of maximum permeability of the rotor:

$$\begin{aligned} \frac{d\lambda_d}{dt} &= v_d - R_s \cdot i_d + \omega_e \cdot \lambda_q; \\ \frac{d\lambda_q}{dt} &= v_q - R_s \cdot i_q - \omega_e \cdot \lambda_d; \\ T &= \frac{3}{2} \cdot Z_p \cdot (L_d - L_q) \cdot i_d \cdot i_q, \end{aligned} \quad (17)$$

where i_d, i_q are the stator currents; v_d, v_q are the stator voltages; λ_d, λ_q are stator flux linkages; $\omega_e = Z_p \cdot \omega_m$ is the electrical angular frequency of the rotor; R_s is the stator resistance; L_d, L_q are the inductances of stator (direct and quadrature).

In both cases the same equation for mechanical speed is used:

$$J \cdot \frac{d\omega_m}{dt} = T - T_L, \quad (18)$$

where J is the moment of inertia; T_L is the load torque.

Parameters of models of the IM and the SynRM in various modes were calculated to obtain the needed values of I_{out} , V_{out} , $\cos\varphi$ of Table 5. First approximations of the parameters were calculated using experimental data (Table 8). Data of no-load and short circuit tests were used for the IM. Data of no-load and rated load tests were used for the SynRM.

Table 8. Electrical parameters of 1.1 kW, 3000 rpm motors.

Parameter	Value
IM	
Line-to-line stator resistance R_s , Ohm (18.4 °C),	9.2
Temperature rise at the rated load, Stator winding (ambient temperature 25 °C), K	40
Line-to-line stator resistance R_s , Ohm (65 °C),	10.8
Main magnetizing inductance L_m , H	0.487
Leakage stator inductance $L_{\sigma s}$, H	0.037
Leakage rotor inductance (referred to stator) $L_{\sigma r}$, H	0.037
Rotor phase resistance (referred to stator) R_r , Ohm	5.95
SynRM	
Line-to-line stator resistance R_s , Ohm (25 °C),	4.5
Temperature rise at the rated load, Stator winding (ambient temperature 25 °C), K	31
Line-to-line stator resistance R_s , Ohm (56 °C),	5.1
Direct stator inductance L_d , H	0.19
Quadrature stator inductance L_q , H	0.035

In order to obtain the electrical load parameters that were needed, new values of L_d and L_q and load torque T were calculated using the SynRM Equations (17). New values of L_m , ω_s and T were obtained in a similar way in case of the IM model. Table 9 shows the calculated parameters of IM and SynRM. Values of load torque of the models (designated as T_L' in the table) are higher than the torque values of Table 2 in the corresponding modes. This is due to the fact that magnetic and mechanical losses are not taken into account in Equations (16) and (17) while the value of active power P_{1ph} is calculated using experimental data (Table 5).

Table 9. Calculated parameters of motors in operating modes of Table 5.

Mode No.	IM			SynRM		
	L_m, H	$\omega_s, rad/s$	$T_L', N \cdot m$	L_d, H	L_q, H	$T_L', N \cdot m$
1	0.47	7.69	1.817	0.243	0.0431	1.609
2	0.482	9.627	2.25	0.233	0.0381	2.029
3	0.505	12.34	2.855	0.199	0.0329	2.592
4	0.555	16.817	3.776	0.185	0.0314	3.445

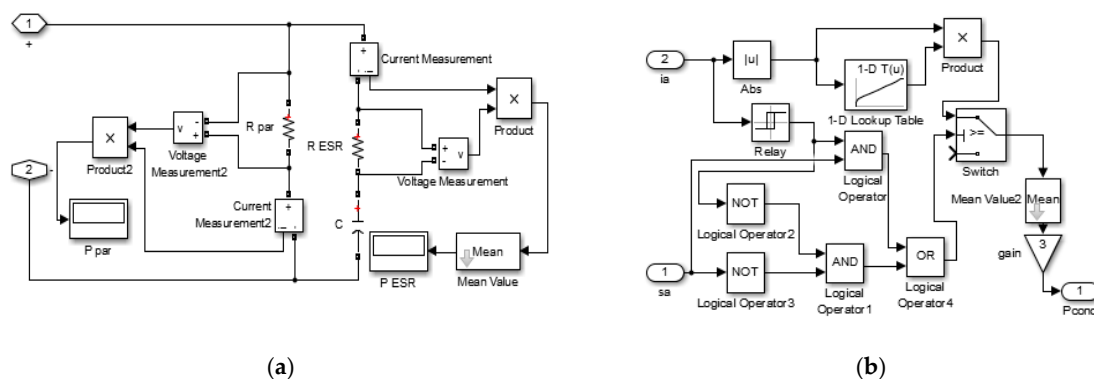
Figure 6a shows the model of CDM with IM. Figure 6b shows the model of CDM with SynRM.

The voltage reference for the PWM controller is set in the fixed coordinate system DQ in case of IM. The DQ voltage reference is set using a current field-oriented control system in case of SynRM [12]. The control system provides the fixed motor current angle $\gamma = \text{atan}(i_q/i_d)$. The reference of current magnitude is provided by the PI controller of the rotational speed ω_m .

The "Delay block 1" is used to implement a discrete delay so that the values of the references V_D^* and V_Q^* do not change during the PWM period. The vector PWM controller is modeled using the standard block "SVPWM Generator (2-Level)" of the "SimPowerSystems" library.

An inverter with ideal switches is modeled using the standard block "Universal bridge" of the "SimPowerSystems" library.

Figure 6c shows the model implemented by the "DC supply" block. The rectifier is modeled using 6 standard blocks "Diode" of the "SimPowerSystems". Figure 7a shows the DC-link model. The same values of R_{par} and R_{ES} parameters are used as for the analytical model. The capacitance $C_{DC\ link} = 1880 \mu F$ was assumed to be equal to the actual capacitance installed in the sample of a serial FC with a power of 1.1 kW.

**Figure 7.** (a) Model of DC-link; (b) IGBT conduction losses calculation.

In order to obtain the correct amplitude of the FC input current RL-branches representing the impedance of the power grid were also added in the model. Values $R_{net} = 0.1 \text{ Ohm}$, $L_{net} = 3.2 \cdot 10^{-5} \text{ H}$ of phase grid impedance were assumed.

The conduction losses are calculated by integrating the instantaneous values of the current $i(t)$ and the voltage drop $\Delta u(i)$. The switching losses are computed by the switch control signals from one of the inverter phases and the instantaneous current values calculated by the model [18]. To calculate the $\Delta u(i)$ values and switching losses, the nonlinear characteristics of the elements are used, see Figure 5, which are set using the "1-D Lookup Table". For example, Figure 7b shows a subsystem that calculates the losses in transistors during ON-state, according to reference [18]. The control and the ventilation losses are taken into account in the same way as for the analytical model.

Figure 8 shows an example of the calculation results using the model. Waveforms of phase motor current, phase motor voltage, phase rectifier input current, DC-link voltage and current of the DC-link capacitance are shown. Instantaneous values are shown by red line. Values averaged over PWM period are shown by blue line. One can notice that the current of the DC-link capacitance has both

low-frequency ripples caused by the FC rectifier stage and high-frequency ripples caused by the FC inverter stage.

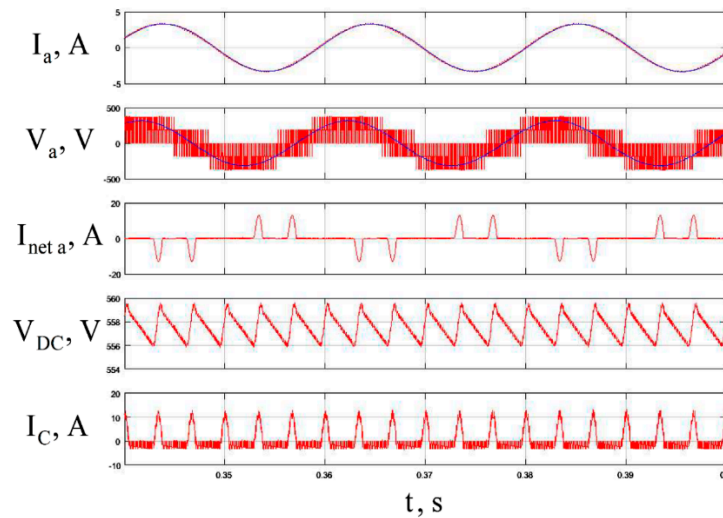


Figure 8. Waveforms of currents and voltages of CDM (Simulink model).

3.3. Comparison of Analytical Calculation and Numerical Simulation Results

In this section the results of losses calculations in CDM using the two methods discussed before are compared. Figures 9 and 10 show a comparison of various types of losses in CDM, calculated by analytical and numerical methods for the IM and SynRM drive for two loading cases; load case 1 is plotted in Figure 8 for mode No 1, while load case 2 is sketched in Figure 9 for mode No. 4 of Table 2.

Figures 9 and 10 have the following designation for motor characteristics: $P_{L on T}$ is the conduction losses in the IGBTs; $P_{L on S}$ is the conduction losses in the reverse diodes; $P_{L sw Ton}$ is the turn-on losses of the IGBTs; $P_{L sw Toff}$ is the turn-off losses of the IGBTs; $P_{L sw D}$ is the turn-off losses of the reverse diodes; $P_{L rect}$ is the losses of the rectifier; $P_{par DC}$ is the losses in the balancing resistors in the DC-link; $P_{cap DC}$ is the losses in the DC-link capacitors.

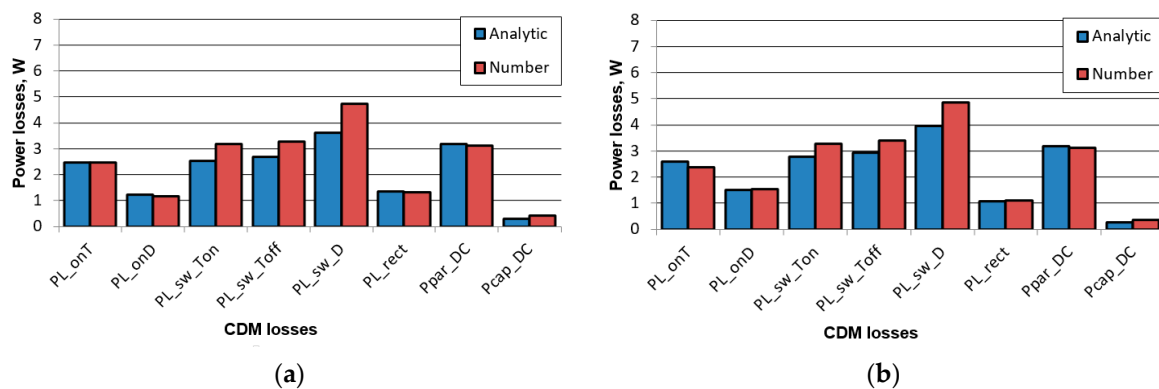


Figure 9. CDM losses using the analytical and the numerical methods for mode No. 1 of Table 2: (a) IM drive; (b) SynRM drive.

Based on Figures 9 and 10, it can be concluded that despite the analytical model having some assumptions and not considering the nonlinearity in the losses, it gives a good matching for the losses calculation in CDM compared to the numerical model that uses more accurate relations. The main causes of errors of the analytical model are inaccuracy of linear interpolation of $V-I$ and $E-I$ characteristics of semiconductor elements and the inaccuracy of calculation of the current values of CDM elements using analytical formulas. The difference in the sum of losses in CDM between both

models is in the range of 0.7–6.9%, depending on the mode under consideration. Thus, the considered analytical model can be used for a comparative assessment of the energy consumption of different configurations of the electric drive.

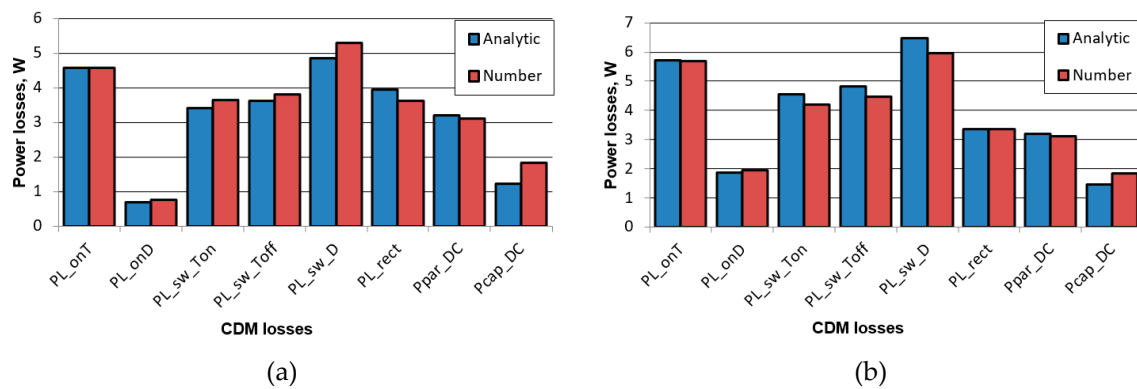


Figure 10. CDM losses by the analytical and the numerical methods for mode No. 4 of Table 2: (a) IM drive; (b) SynRM drive.

3.4. Comparison of Analytical Calculation and Experimental Results

During tests of the SynRM not only were currents and voltage at the output of the FC being measured, but also the electric values at the FC input. Therefore, in this case we have the opportunity to compare the calculated losses and the measured ones. A general purpose FC with the rated power of 1.5 kW and a sensorless control method for SynRM were used for this test (Figure 11a) [27].

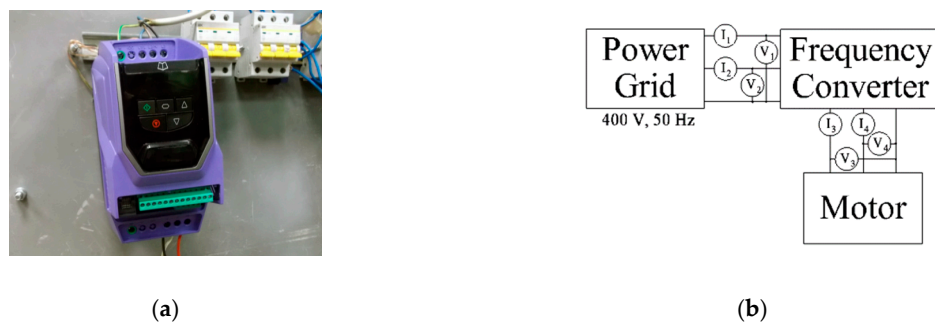


Figure 11. Converter testing: (a) Photograph of the FC; (b) Scheme of the test, I_1 – I_4 are current sensors; V_1 – V_4 are voltage sensors.

In order to measure the electric values, the LEM sensors (CV 3-1000 and LA 25 NP at the FC output, LV 25-P/SP-5 and LA 25 NP at the FC input) are used. The signals coming from the sensors are recorded using the analog-to-digital converter QMBox20-16 (Figure 11b). The voltage sensors applied (CV 3-1000) have a wide frequency bandwidth (up to 500 kHz) and are suitable to measure the PWM voltage. In addition, we use a high enough sample rate of ADC (300 kHz) and averaging the results during a large number of fundamental electrical periods. CDM losses were measured in 7 operating points specified in Table 4 for the case of SynRM testing.

In previous sections separate components of CDM losses were calculated. However, it is not so easy to carry out experimental results for the separate components. It requires installing a large number of suitable sensors in the inner schematics of the converter and taking into account energy losses in the sensors. Therefore, in this work experimental data of sum of CDM losses are presented.

Figure 12 shows the comparison of CDM losses calculated by the analytical method and measured during the test. It can be seen that the calculated and measured losses are in a good agreement. Some differences can be explained by inaccuracy of the parameters of the model applied.

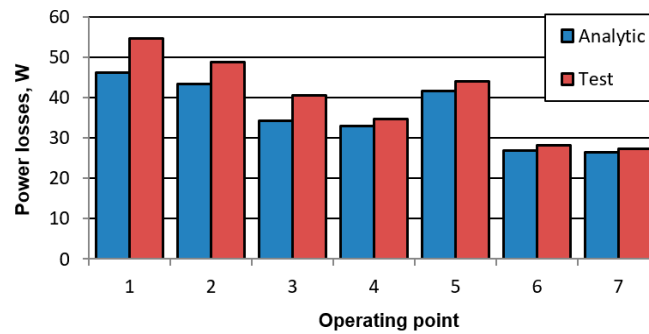


Figure 12. CDM losses by the analytical method and by the experiment for 7 operating points according Table 4 in case of SynRM.

4. Efficiency and Losses Calculation for Drives with Different Types of Motor

As shown in the previous section, calculating the sum of losses in CDM using both analytical and numerical methods under consideration provides corresponding results. Therefore, to compare the energy characteristics of electric drives with IM and SynRM, the authors use the analytical model because it has a reduced computation time.

Figure 13 shows the ratio of different types of losses in CDM using different types of motors for the high loaded case (Mode No. 4). Losses in ON-state transistors ($P_{L_{onT}}$) and ON-state reverse diodes ($P_{L_{onD}}$) are distributed depending on the motor power factor (the higher the $\cos\varphi$ is, the higher the loss share in the transistors is). Losses in rectifier diodes ($P_{L_{rect}}$) decrease with the increasing motor efficiency.

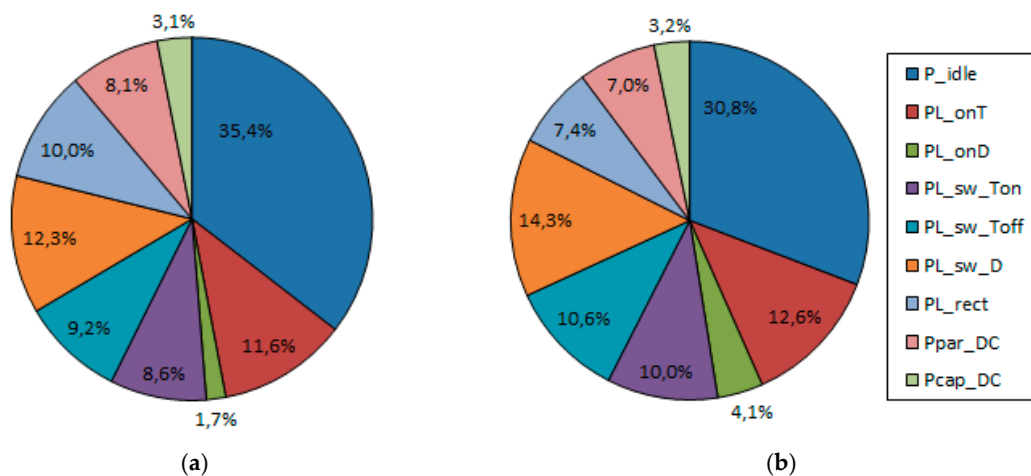


Figure 13. CDM Loss components in mode 4 for different motor types: (a) IM (total loss value 39.5 W); (b) SynRM (total loss value 45.4 W).

For mode No. 4, the sum of losses in the CDM for IM is 39.5 W, and it is 45.4 W for SynRM. Thus, the use of SynRM causes an increase in CDM losses of 14.9%.

Figure 14 shows a comparison of total CDM losses with IM and SynRM for all modes under consideration.

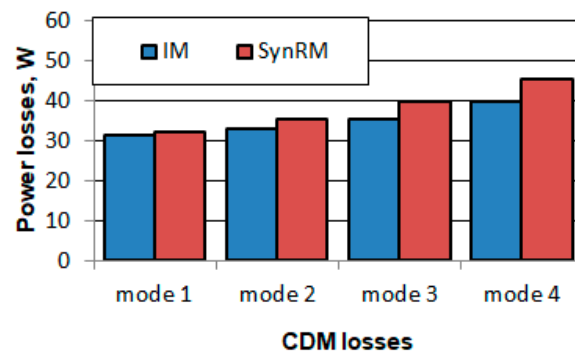


Figure 14. CDM losses for different types of motor in various modes.

Figure 15 shows the calculated efficiencies of CDM, motors, and drives in cases of IM and SynRM. The results for the motors (Figure 15b) are shown in Table 5. The obtained results show that, despite the decrease in the CDM efficiency with the SynRM of about 1%, the efficiency of the SynRM drive is higher than the efficiency of the IM drive by 7.9–11.5%, depending on the load case (Figure 15c).

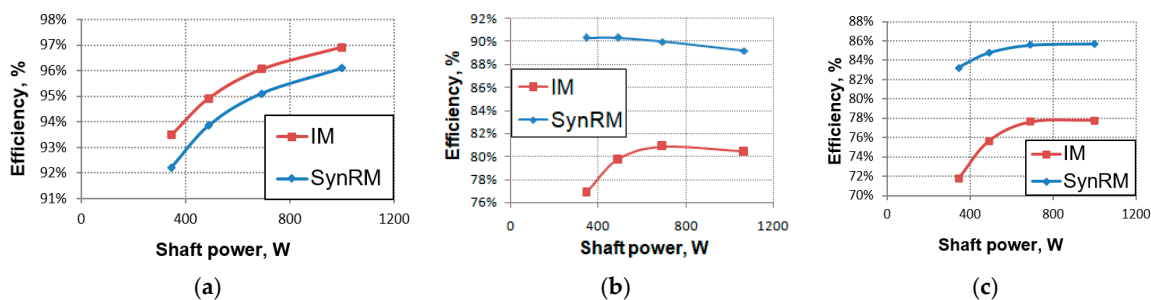


Figure 15. Calculated efficiency: (a) CDMs; (b) Motors; (c) Drives.

Figure 16 shows the ratio of losses in the motor and converter for various cases. It can be seen that when using SynRM the share of losses in CDM from the total losses of the drive is significantly higher due to the reduction of losses in the motor. This illustrates the importance of loss optimization in CDM for a SynRM drive.

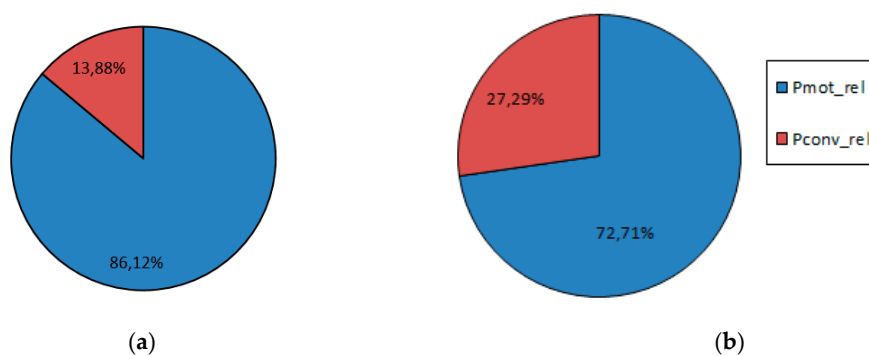


Figure 16. Loss components in mode 4: (a) IM drive; (b) SynRM drive.

Let us also calculate the power consumption of the considered drive configurations in the pump load cycle (Table 2). Figure 17a shows the power values of P_1 , consumed from the power grid by IM and SynRM drives in various modes, as well as the relative duration of these modes. Figure 17b shows the daily energy consumption in the same modes. The total energy consumption of drives with IM and SynRM per one year is 5710 kWh and 5060 kWh respectively. Using SynRM leads to an energy savings of about 12.8% compared to IM. This results in an annual energy saving of about 128 € with the electricity tariff of € 0.1969/kW hour (price for the industry in Germany [34]).

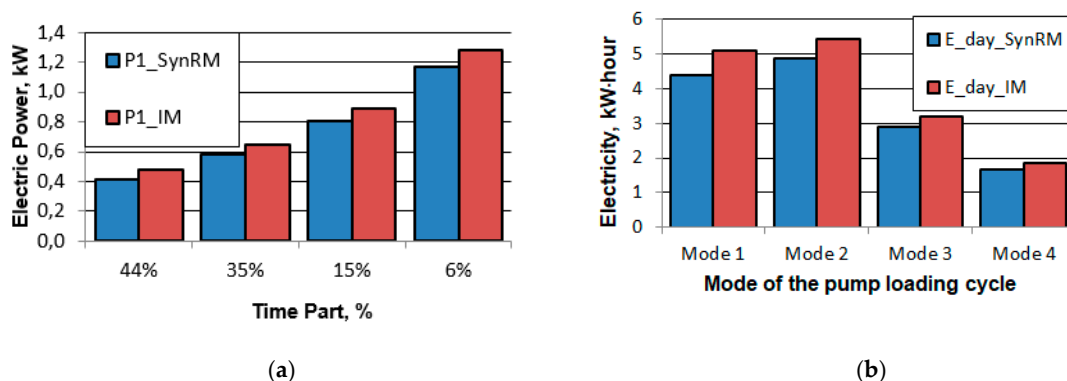


Figure 17. (a) Power consumption by various types of drive in the pump load cycle; (b) Energy consumption per day by various types of drive in the pump load cycle.

5. Conclusions

In this paper, the energy losses in variable speed electric drives for pump applications employing induction and synchronous reluctance motors (IM and SynRM) have been investigated. Extensive mathematical models, simulations and experimental measurements have been carried out for the drive system using both SynRM and IM. The losses in the frequency converter have been calculated using both proposed analytical and numerical models, while considering more accurate relations. The obtained calculated losses of the analytical and the numerical methods correspond; hence the proposed analytical model would be preferred in the simulations because of the low computation time.

It is observed that the losses in the complete drive module (CDM) using SynRM are higher by about 14.9% than when using IM. This is due to the higher current of SynRM, as a result of a lower power factor, resulting in a decrease in the CDM efficiency. However, thanks to the remarkable higher SynRM efficiency, the total efficiency of the SynRM drive is higher than that of the IM by about 7.9%–11.5%. This amount of increase in the efficiency of SynRM drive depends on the loading case; it is even greater for partial loads, which involve the typical operation of pumps, fans, blowers and compressors.

Moreover, the study shows that the annual energy saving using SynRM drive is higher by about 12.8% compared to IM, but the installation cost of SynRM drive might be higher due to mainly the higher converter rating. Eventually, it can be concluded that using SynRM drives for pump applications decreases the lifetime costs thanks to the lower energy consumption.

In future work, the influence of control methods of IM and SynRM on the energy consumption of pump applications will be investigated.

Author Contributions: All the authors contributed substantially to the manuscript. Contributions of each author are as follows: conceptual approach, V.P. and V.D.; calculations and modeling, V.K. and V.P.; experiments, V.K. and S.O.; writing of original draft, V.K., V.P. and V.D.; visualization, V.K., V.P., V.D., M.N.I., S.O. and S.S.; review and editing, M.N.I., S.O. and S.S.

Funding: The research was conducted on theme no. 8.9549.2017/8.9. within the frame of the government task of the Ministry of Education and Science of the Russian Federation in R&D.

Conflicts of Interest: The authors declare no conflict of interest.

References

1. Commission Regulation (EC) No 640/2009 Implementing Directive 2005/32/EC of the European Parliament and of the Council with Regard to Ecodesign Requirements for Electric Motors. Available online: <https://eur-lex.europa.eu/legal-content/EN/TXT/PDF/?uri=CELEX:32009R0640&from=FR> (accessed on 21 December 2018).
2. *Rotating Electrical Machines—Part 30-2: Efficiency Classes of Variable Speed AC Motors (IE-Code)*; IEC 60034-30-2/Ed1; IEC: Geneva, Switzerland, 2016.

3. USDOE. *Energy Savings Potential and Opportunities for High Efficiency Electric Motors in Residential and Commercial Equipment*; Department of Energy: Washington, DC, USA, 2013. Available online: <https://www.energy.gov/sites/prod/files/2014/02/f8/Motor%20Energy%20Savings%20Potential%20Report%202013-12-4.pdf> (accessed on 21 December 2018).
4. Stoffel, B. *Assessing the Energy Efficiency of Pumps and Pump Units. Background and Methodology*; Elsevier: Amsterdam, The Netherlands, 2015.
5. *Adjustable Speed Electrical Power Drive Systems—Part 9-2: Ecodesign for Power Drive Systems, Motor Starters, Power Electronics and Their Driven Applications—Energy Efficiency Indicators for Power Drive Systems and Motor Starters*; IEC 61800-9-2/Ed1; IEC: Geneva, Switzerland, 2017.
6. Aarniovuori, L.; Musikka, T.; Kosonen, A.; Niemelä, M.; Pyrhönen, J. Three alternative methods to determine voltage source converter losses. In Proceedings of the 2015 17th European Conference on Power Electronics and Applications (EPE'15 ECCE-Europe), Geneva, Switzerland, 8–10 September 2015; pp. 1–10.
7. Ahonen, T.; Orozco, S.; Ahola, J. Effect of electric motor efficiency and sizing on the energy efficiency in pumping systems. In Proceedings of the International Conference on Power Electronics and Applications (EPE'16 ECCE Europe), Karlsruhe, Germany, 5–9 September 2016; pp. 1–9.
8. Vartanian, R.; Deshpande, Y.; Toliyat, H. Performance Analysis of a Ferrite Based Fractional Horsepower Permanent Magnet Assisted SynRM for Fan and Pump Applications. In Proceedings of the International Conference on Electric Machines & Drives Conference (IEMDC 2013), Chicago, IL, USA, 12–15 May 2013; pp. 1405–1410. [[CrossRef](#)]
9. Safin, N.; Kazakbaev, V.; Prakht, V.; Dmitrievskii, V. Calculation of the Efficiency and Power Consumption of Induction IE2 and Synchronous Reluctance IE5 Electric Drives in the Pump Application Based on the Passport Specification According to the IEC 60034-30-2. In Proceedings of the 25th International Workshop on Electric Drives: Optimization in Control of Electric Drives (IWED 2018), Moscow, Russia, 31 January–2 February 2018; pp. 1–5. [[CrossRef](#)]
10. Boglietti, A.; Cavagnino, A.; Pastorelli, M.; Vagati, A. Experimental comparison of induction and synchronous reluctance motors performance. In Proceedings of the 40th IEEE IAS Annual Meeting, Kowloon, Hong Kong, China, 2–6 October 2005; pp. 474–479.
11. Doğru, U.; Özçelik, N.; Gedik, H.; İmeryüz, M.; Ergene, L. Numerical and Experimental Comparison of TLA Synchronous Reluctance Motor and Induction Motor. In Proceedings of the 2016 IEEE International Power Electronics and Motion Control Conference (PEMC 2016), Varna, Bulgaria, 25–28 September 2016; pp. 619–624. [[CrossRef](#)]
12. Moghaddam, R.; Magnussen, F.; Sadarangani, C. Theoretical and Experimental Reevaluation of Synchronous Reluctance Machine. *IEEE Trans. Ind. Electron.* **2010**, *57*, 6–13. [[CrossRef](#)]
13. Pina, A.; Xu, L. Comparison of apparent power consumption in Synchronous Reluctance and Induction Motor under vector control. In Proceedings of the Transportation Electrification Conference and Expo (ITEC 2015), Dearborn, MI, USA, 14–17 June 2015; pp. 1–6.
14. Lang, K.; Muetze, A.; Bauer, R.; Pircher, S. Comparison of induction and synchronous reluctance machine based actuators for elevated temperature environments. *IEEE Trans. Energy Convers.* **2016**, *31*, 1012–1022. [[CrossRef](#)]
15. Fratta, A.; Vagati, A.; Villata, F. On the evolution of AC machines for spindle drive applications. *IEEE Trans. Ind. Appl.* **1992**, *28*, 1081–1086. [[CrossRef](#)]
16. Bierhoff, M.; Fuchs, F. Semiconductor losses in voltage source and current source IGBT converters based on analytical derivation. In Proceedings of the 2004 IEEE 35th Annual Power Electronics Specialists Conference (IEEE Cat. No.04CH37551), Aachen, Germany, 20–25 June 2004; pp. 2836–2842. [[CrossRef](#)]
17. Muhammad, H. *Power Electronics Handbook: Devices, Circuits, and Applications*; Butter Worth Heinemann, Elsevier: Burlington, NJ, USA, 2011.
18. Pou, J.; Osorno, D.; Zaragoza, J.; Jaen, C.; Ceballos, S. Power losses calculation methodology to evaluate inverter efficiency in electrical vehicles. In Proceedings of the 2011 7th International Conference-Workshop Compatibility and Power Electronics (CPE 2011), Tallinn, Estonia, 1–3 June 2011; pp. 404–409. [[CrossRef](#)]
19. Suh, Y.; Steinke, J.; Steimer, P. Efficiency Comparison of Voltage-Source and Current-Source Drive Systems for Medium-Voltage Applications. *IEEE Trans. Ind. Electron.* **2007**, *54*, 2521–2531. [[CrossRef](#)]

20. Hajizadeh, A. Optimized Thermal Management System of Modular Multilevel Converter for HVDC applications. In Proceedings of the 2017 IMAPS Nordic Conference on Microelectronics Packaging (NordPac), Gothenburg, Sweden, 18–20 June 2017; pp. 1–5. [CrossRef]
21. Laprade, A.; Randall, R. Numerical Method for Evaluating IGBT Losses, Application Note, Fairchild Semiconductor, AN-7520, Rev. A1. January 2000. Available online: <https://www.fairchildsemi.com/application-notes/AN/AN-7520.pdf> (accessed on 21 December 2018).
22. NM, NMS, Close Coupled Centrifugal Pumps with Flanged Connections; Catalogue; Calpeda. 2018. Available online: https://www.calpeda.com/system/products/catalogue_50hzs/53/en/NM_NMS_EN2018.pdf?1549893188 (accessed on 23 March 2019).
23. Doppelbauer, M. Interpolation Procedures for the Determination of Losses and Energy Efficiency of Electrical Machines. In Proceedings of the Energy Efficiency in Motor Driven Systems, Helsinki, Finland, 15–17 September 2015.
24. Dmitrievskii, V.; Prakht, V.; Kazakbaev, V.; Oshurbekov, S.; Sokolov, I. Developing ultra premium efficiency (IE5 class) magnet-free synchronous reluctance motor. In Proceedings of the 6th International Electric Drives Production Conference (EDPC 2016), Nuremberg, Germany, 30 November–1 December 2016; pp. 1–6. [CrossRef]
25. Type: M3AA 80 C 2, Type Test Reoprt, ABB Group, 3GE114080T1102, 2011.12.19. Available online: https://library.e.abb.com/public/ca860f63c15d41a6c12579f4003a7166/M3AA80C2_G_3GAA081443_E.pdf (accessed on 18 January 2019).
26. *Rotating Electrical Machines—Part 2-3: Specific Test Methods for Determining Losses and Efficiency of Converter-Fed AC Induction Motors*; IEC 60034-2-3/Ed1; IEC: Geneva, Switzerland, 2013.
27. *Optidrive P2, AC Variable Speed Drive, 0.75 kW–250 kW / 1HP–350HP, 200–480 Volt 1 & 3 Phase; Advanced User Guide, Revision 1.00*; Invertek Drives Ltd.: Buttington, UK, 2012; Available online: <https://www.invertekdrives.com/client-uploads/download-manager/user-guides/Optidrive%20P2%20Advanced%20User%20Guide%20Rev%201.00.pdf> (accessed on 23 March 2019).
28. KSB SuPremE in IE5: The World’s Most Efficient Magnet-less Pump Motor. Available online: <https://www.ksb.com/blob/1359690/72681a8b4176a7d1f38b8cfe26cd50e7/supreme-ie5-en-data.pdf> (accessed on 21 December 2018).
29. FP25R12W2T4_B11, IGBT-Modules, Technical Information, Revision 2.1, Infineon. November 2013. Available online: https://www.infineon.com/dgdl/Infineon-FP25R12W2T4_B11-DS-v02_01-en_de.pdf?fileId=db3a30431add1d95011aed27bf4a0232 (accessed on 21 December 2018).
30. Calculation of Conduction Losses in a Power Rectifier, Application Note, STMicroelectronics Group of Companies, AN-604, Document ID 3607, Revision 3. August 2011. Available online: https://www.st.com/resource/en/application_note/cd00003894.pdf (accessed on 6 December 2018).
31. Orfanoudakis, G.; Sharkh, S.; Yuratich, M. Analysis of DC-Link Capacitor Losses in Three-Level Neutral Point Clamped and Cascaded H-Bridge Voltage Source Inverters. *IEEE Trans. Ind. Electron.* **2014**, *61*, 3099–3108. [CrossRef]
32. Kolar, J.; Round, S. Analytical calculation of the RMS current stress on the DC-link capacitor of voltage-PWM converter systems. *IEE Proc. Electr. Power Appl.* **2006**, *153*, 535–543. [CrossRef]
33. HMAX Variable Frequency Drive Watt Loss Data at Operation Load Levels, Application Note, Eaton, AP040125EN. March 2016. Available online: http://www.eaton.ec/EN/ecm/idcplg?IdcService=GET_FILE&allowInterrupt=1&RevisionSelectionMethod=LatestReleased&noSaveAs=0&Rendition=Primary&dDocName=AP040125EN (accessed on 21 December 2018).
34. Eurostat Data for the Industrial Consumers in Germany. Available online: http://ec.europa.eu/eurostat/statistics-explained/index.php/Electricity_price_statistics#Electricity_prices_for_industrial_consumers (accessed on 21 December 2018).

